Biosensors and Bioelectronics 82 (2016) 204–211

Contents lists available at ScienceDirect

Biosensors and Bioelectronics

journal homepage: www.elsevier.com/locate/bios

Fluorescence "turn-on" determination of H_2O_2 using multilayer porous SiO_2/NGQDs and PdAu mimetics enzymatic/oxidative cleavage of single-stranded DNA

Linlin Liang [a], Feifei Lan [a], Li Li [a], Min Su [a], Shenguang Ge [a,b,*], Jinghua Yu [a], Haiyun Liu [a], Mei Yan [a]

[a] School of Chemistry and Chemical Engineering, University of Jinan, Jinan 250022, PR China
[b] Shandong Provincial Key Laboratory of Preparation and Measurement of Building Materials, University of Jinan, Jinan 250022, PR China

ARTICLE INFO

Article history:
Received 31 January 2016
Received in revised form
30 March 2016
Accepted 30 March 2016
Available online 1 April 2016

Keywords:
Fluorescence
Hollow channels
Nitrogen-doped graphene quantum dots
PdAu mimetics enzymatic
Visualization

ABSTRACT

A 3D microfluidic paper-based fluorescence analytical device with hollow channels based on the turn-on switching of a resonance energy transfer triggered by the •OH induced cleavage of a DNA strand was successfully constructed. And this fluorescent nanoplatform was first designed to achieve in situ and real-time determination of H_2O_2 released from cancer cells to obtain an accurate determination. With optimal conditions, the proposed method displayed excellent analytical performance for the detection of H_2O_2 ranging from 0.3 to 1.0 mM with a detection limit of 0.1 nM. The favorable performances of this sensor were due to the peroxidase-like activity of nitrogen-doped graphene quantum dots (multilayer porous SiO_2 act as stabilizer to load more nitrogen-doped graphene quantum dots for signal amplification) and folic acid-pPdAu/GO (which also could act as an efficient fluorescence quencher and a recognition element of cancer cells by folic acid). It was worth noting that it could be used for visually determined the flux of H_2O_2 from the cells. Therefore, the developed biosensor holds potential for ultrasensitive quantitative analysis of H_2O_2 and supplies valuable information for diabetes mellitus research and clinical diagnosis.

1. Introduction

Hydrogen peroxide (H_2O_2), a major reactive oxygen species (ROS) in living systems, which is important intracellular signaling molecules, mainly regulating DNA damage, protein synthesis, cell apoptosis, etc (Zhang et al., 2013; Chang et al., 2013; Sanford et al., 2010; Shibutani et al., 1991; Kanvah et al., 2010). It is the most common representative of ROS studied in cellular environments because its stability allows it to penetrate cellular membranes into other cellular compartment to potentially induce various harmful biological modifications. Therefore, selective and quantitative detection of the level of intracellular H_2O_2 is of great value in elaborating its regulation of signal transduction pathways and searching for new therapeutic strategies for cancer and other diseases. A variety of chemical tools, including mass probes (Cocheme et al., 2012), proteomics probes (Belousov et al., 2006), and fluorescent probes (Lippert et al., 2011), and so on, have been developed for determining cellular H_2O_2. Although, among these probes, fluorescent probes have been widely studied because of their fast response for analysis and nondisruptive features. There is still an urgent need for a visual, facile, portable, disposable and low-cost detection for the sensitive and selective profiling of H_2O_2, especially in developing countries, resource-limited and remote regions.

Microfluidic paper-based analytical devices (μPADs) were firstly reported by Whiteside's group (Martinez et al., 2007) as promising platforms designed for point-of-care diagnosis. Thereafter, increasing attention has been paid to μPADs because of its attractive features including low cost, ease of use, low consumption of reagents and samples, and so on (Martinez et al., 2010; Whitesides et al., 2006). Importantly, μPADs are easily fabricated in bulk using waxprinting. So, many groups have paid great efforts to the development of μPADs (Liu and Crooks, 2012; Ge et al., 2013). Up to now, colorimetric detection is the most commonly used assay method on μPADs, the fluorescence assay is another kind of optical method possessing inherently much higher sensitivity than colorimetric methods (Yetisen et al., 2013; Nery et al., 2013). More recently, instead of cellulose network, μPADs with hollow channels for fluids transport have been demonstrated (Renault et al., 2013),

* Corresponding author at: School of Chemistry and Chemical Engineering, University of Jinan, Jinan 250022, PR China.
E-mail address: chm_gesg@163.com (S. Ge).

http://dx.doi.org/10.1016/j.bios.2016.03.076
0956-5663/

which possesses the distinguished advantage of easy fabrication, with no pump requirement and that enable rapid fluid flow (Renault et al., 2014). Inspired by this simple technique, a 3D microfluidic paper-based fluorescence analytical device with hollow channels (HC-PFAD) was demonstrated based on origami principle using wax-patented technology and laser cut.

To further perform high-performance, sensitivity enhanced fluorescence assays for H_2O_2 detection, more attention has been focused on nanomaterials and popular strategies for signal amplification. Graphene quantum dots (GQDs) have attracted more researchers because of their robust biological and chemical inertness, tunable luminescence emission, low cytotoxicity, excellent biocompatibility, and resistance to photobleaching (Li et al., 2013; Lin et al., 2014). Meanwhile, both theoretical study and experimental results have proved that heteroatom doped GQDs can offer more active sites and favorable catalytic performance on H_2O_2 reduction (Lin et al., 2015). Up to now, the nitrogen-doped GQDs (NGQDs) have become headline-grabbing studies. Recently, Lai utilized the wide band gap of mesoporous silica to synthesize mesoporous silica-CdS composite, which showed higher signal, lower applied potential and better stability (Lai et al., 2003) than CdS QDs. Similarly, multilayer porous SiO_2 ($MPSiO_2$) with both large surface area and hollow structure have been successfully prepared in this paper to load more NGQDs as well as to modify NGQDs (named $MPSiO_2$/NGQDs nanocomposites) for signal amplification. We demonstrate this DNA mediated self-assembled strategy can not only enhance the quenching efficiency but also improve the stability of $MPSiO_2$/NGQDs. To produce a fluorescence "turn on" detection strategy, grapheme oxide (GO) is selected as a superquencher to probe fluorescence first. To date, GO can act as an efficient fluorescence quencher based on the photoinduced electron transfer mechanism or energy transfer mechanism. GO interacts with single-stranded DNA (ssDNA) through π-π stacking interaction with nucleobases and efficiently quenches fluorescence of QDs (He et al., 2010; Chou et al., 2012). Recently, it was reported that some noble metal nanomaterials possessed intrinsic peroxidase-like activity (Su et al., 2012). Owing to the synergistic effect and the electronic effect, bimetallic nanoalloys have been demonstrated to exhibit improved catalytic performance, the dendritic/porous nanostructures are beneficial to high catalytic performance (Lim and Xia, 2011), because of their high surface area and rich surface atoms. Based on the above concept, folic acid (FA)-pPdAu/GO as mimicking natural peroxidases were fabricated, which also could act as an efficient fluorescence quencher and a recognition element of cancer cells by folic acid.

Herein, we fabricated a novel non-enzymatic approach for measuring the release of H_2O_2 from living cancer cells (using the MCF-7 cancer cell as a model) based on the fluorescence turn-on detection of non-enzymatic cleavage of single-stranded DNA with high sensitivity and selectivity. Compared with the previously reported fluorescence-based H_2O_2 detection strategies (Shang and Dong 2009; Dickinson et al., 2008), our proposed method possessed some remarkable features: firstly, as a type of green environment-friendly FA-pPdAu/GO nanocatalysts, which not only exhibited an excellent peroxidase-like activity but also could act as an efficient fluorescence quencher through π-π stacking interaction with ssDNA and a recognition element of cancer cells by folic acid. Secondly, self-assembly $MPSiO_2$ could act as signal amplifier. the produced NGQDs as the fluorescence report element could ensure ideal signal output because of the long-term photo stability, which also presented intrinsic peroxidase-like activity. thirdly, the DNA could be cleaved by hydroxyl radical (•OH) produced by the reaction between three peroxidase-like nanocatalysts and H_2O_2. Most importantly, this assay was easy to implement for visual detection with the assistance of a UV light in HC-μPADs. In addition, this sensing system was generalizable and could further extended to the detection of H_2O_2-involved analytes such as glucose and acetylcholine. Therefore, this approach was not only sensitive and selective but also convenient and generalizable.

2. Experimental section

2.1. Fabrication of the HC-μPADs

The materials and apparatus were shown in Supporting information. The HC-μPADs were fabricated using a previously reported wax patterning method (Carrilho et al., 2009; Renault et al., 2014) with large modifications and a detailed procedure was described below (details in Supporting information). The schematic representation, size and shape of this HC-μPADs were shown in Scheme S1, Fig. S1–S3.

2.2. Preparation of porous FA-PdAu/GO

The in situ preparation of porous PdAu/GO (pPdAu/GO) was performed according to the method reported previously (Zhang et al., 2014). The detailed preparation process for FA-PdAu/GO was provided in the Supporting information.

2.3. Preparation of NGQDs, $MPSiO_2$ and $MPSiO_2$/NGQDs-DNA

The detailed preparation process for NGQDs, $MPSiO_2$ and $MPSiO_2$/NGQDs-DNA were provided in the Supporting information.

2.4. Detection of the flux of H_2O_2 releasing from cells

Our work aimed at developing a biosensor for monitoring the release process and measuring the flux of H_2O_2 from cells, which was shown schematically in Scheme 1. To demonstrate the feasibility of the proposed detection method. Firstly, the FA-pPdAu/GO (125 μg mL^{-1}) in incubation buffer (PBS, pH 7.4) was added to paper cell zones to act as an efficient fluorescence quencher and a recognition element of cancer cells by folic acid, and then the fluorescent probe (100 μL, respectively) was applied to each paper zone and incubated for 5 min at room temperature. After carefully and thoroughly washing with pH 7.4 PBS. After that, the fluorescence responses of the proposed biosensor toward the various concentrations of H_2O_2 were studied. As shown in Scheme S1, the paper auxiliary tab was folded up above the paper cell tab, then this HC-PFAD was gripped to make them stacked closely. Subsequently, due to the toxic of PMA, so, 100 mg mL^{-1} of PMA was added to pretreatment zone to avoid prolonged cell contact with PMA. Finally, a series of different doses of cells were respectively droped into the centre zone and reacted at 37 °C for 30 min (Fig. S7). Then, the fluorescence was also measured under excitation at 415 nm.

3. Results and discussion

3.1. Characterization of FA-PdAu/GO

The green synthesis of FA-pPdAu/GO included two steps. Firstly, pPd/GO was fabricated by in situ growth with GO with Na_2PdCl_4 at 80 °C for 24 h. Then, the prepared pPd/GO were used as precursors to react with a $HAuCl_4$ solution by galvanic replacement reaction. Since the standard reduction potential of the $AuCl^{4-}$/Au (0.99 V vs standard hydrogen electrode, SHE) is higher than that of the Pd^{2+}/Pd (0.915 V vs SHE), as a result, the loaded Pd atoms were oxidized into Pd^{2+} with the addition of $HAuCl_4$ in

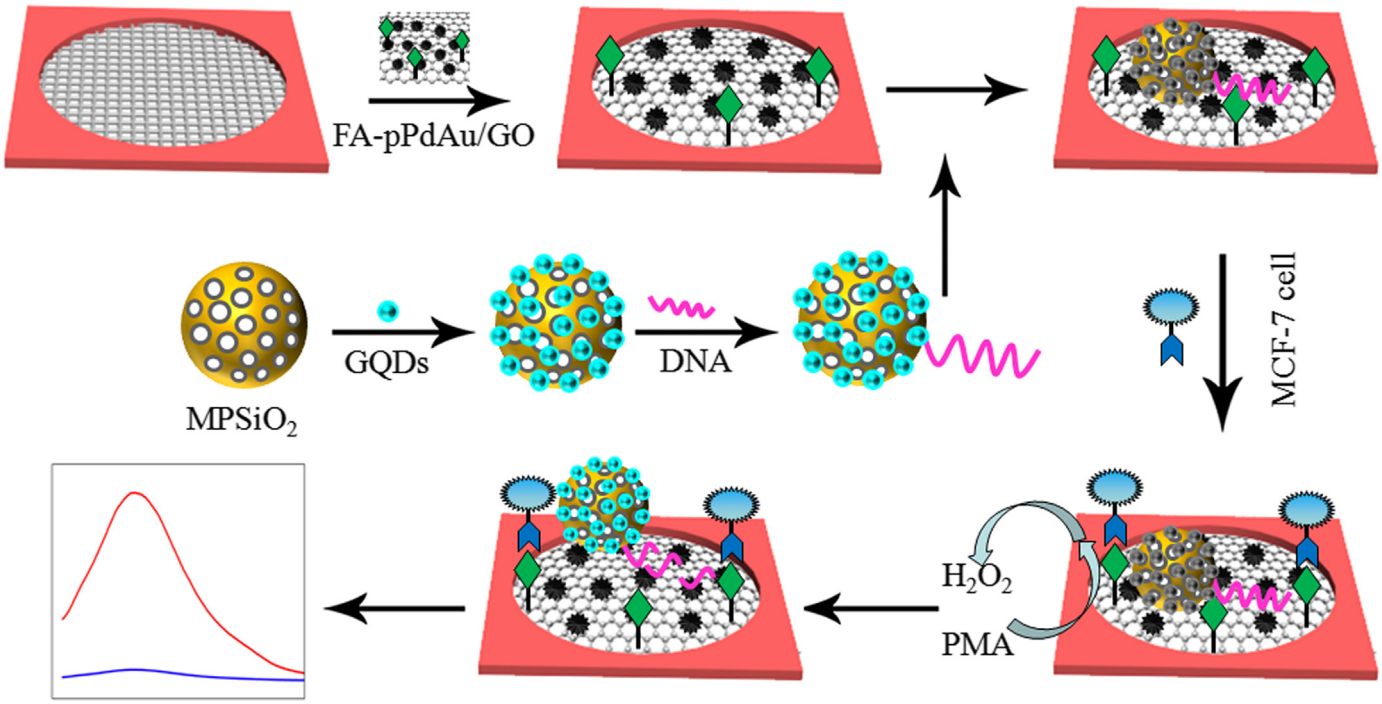

Scheme 1. The schematic representation of the fabrication procedure for H_2O_2 biosensor on HC-μPADs.

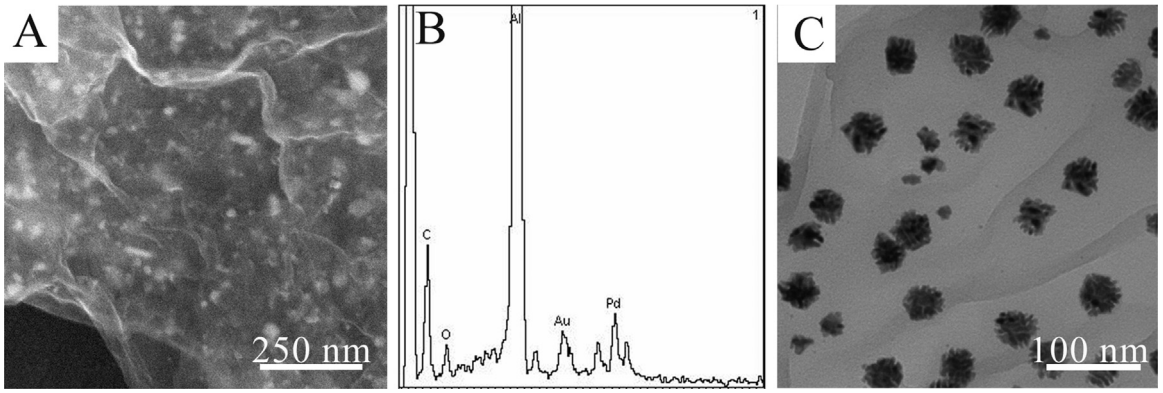

Fig. 1. (A) SEM images of FA-pPdAu/GO. (B) EDS of FA-pPdAu/GO. (C) TEM images of FA-pPdAu/GO.

aqueous solution, Au atoms could replace the Pd atoms on the surface of Pd (Liu et al., 2009; Lee et al., 2005). To verify the successful growth of pPdAu on graphene oxide sheets, SEM and TEM images were used to characterize the morphologies of the as-prepared composites (Fig. 1A,C). A large number of pPdAu with a size of about 40 nm were well-dispersed on the surface of the graphene oxide nanosheets, which should be attributed to the hydroxyl, epoxide, and carboxylic groups uniformly existing on the GO. An EDS spectrum was also used to analyze the elemental distribution of the nanocomposite. The significant Pd and Au signals suggested that the nanoparticles loaded on the surface of graphene oxide were Pd and Au (Fig. 1B), verifying again the successful formation of pPdAu on the GO surface. The purified FA-pPdAu/GO (Fig. S4 and S5) were stored in refrigerator for further characterization and application.

3.2. Characterization of NGQDs, $MPSiO_2$, $MPSiO_2$/NGQDs

As a signal report element, the morphology of the as-prepared NGQDs was first characterized using TEM. TEM characterization of the NGQDs (Fig. 2A) suggested that the as-prepared NGQDs had a good dispersibility and a narrow distribution of diameters in the range of 4–5 nm. To further characterize the composition of NGQDs, XPS was performed. The full scan XPS spectrum of the NGQDs (Fig. S6B) showed the existence of carbon (C 1s, 285 eV), nitrogen (N 1s, 400 eV), and oxygen (O 1s, 533 eV), which confirmed the graphitic structure of NGQDs. Due to the introduction of N atoms owning five valence electrons into benzene ring atoms, the spin density and the charge distribution of the carbon atoms were influence efficiently. So, the density of the catalytically active centers on the graphene surface with low stereohindrance for binding redox species in catalytic reactions was enhanced (Tang et al., 2009). Next, we investigated the optical properties of NGQDs, fluorescence and UV–vis absorption spectra were studied (Fig. S6A). Firstly, For the UV–vis absorption of NGQDs, the NGQDs showed a well-defined absorption band at 360 nm with a narrow full width at half maximum of 50 nm, which further confirmed that the sp^2 hybridization contained in NGQDs should be uniform in size, and the NGQDs also exhibited an excitation dependent fluorescence behavior. With the excitation wavelength changed from 280 to 400 nm (inset), the fluorescence peak shifted to longer wavelengths with the strongest peak at 441 nm when excited at 360 nm. So, we chose 360 nm as the excitation wavelength. And the NGQDs aqueous solutions exhibited blue

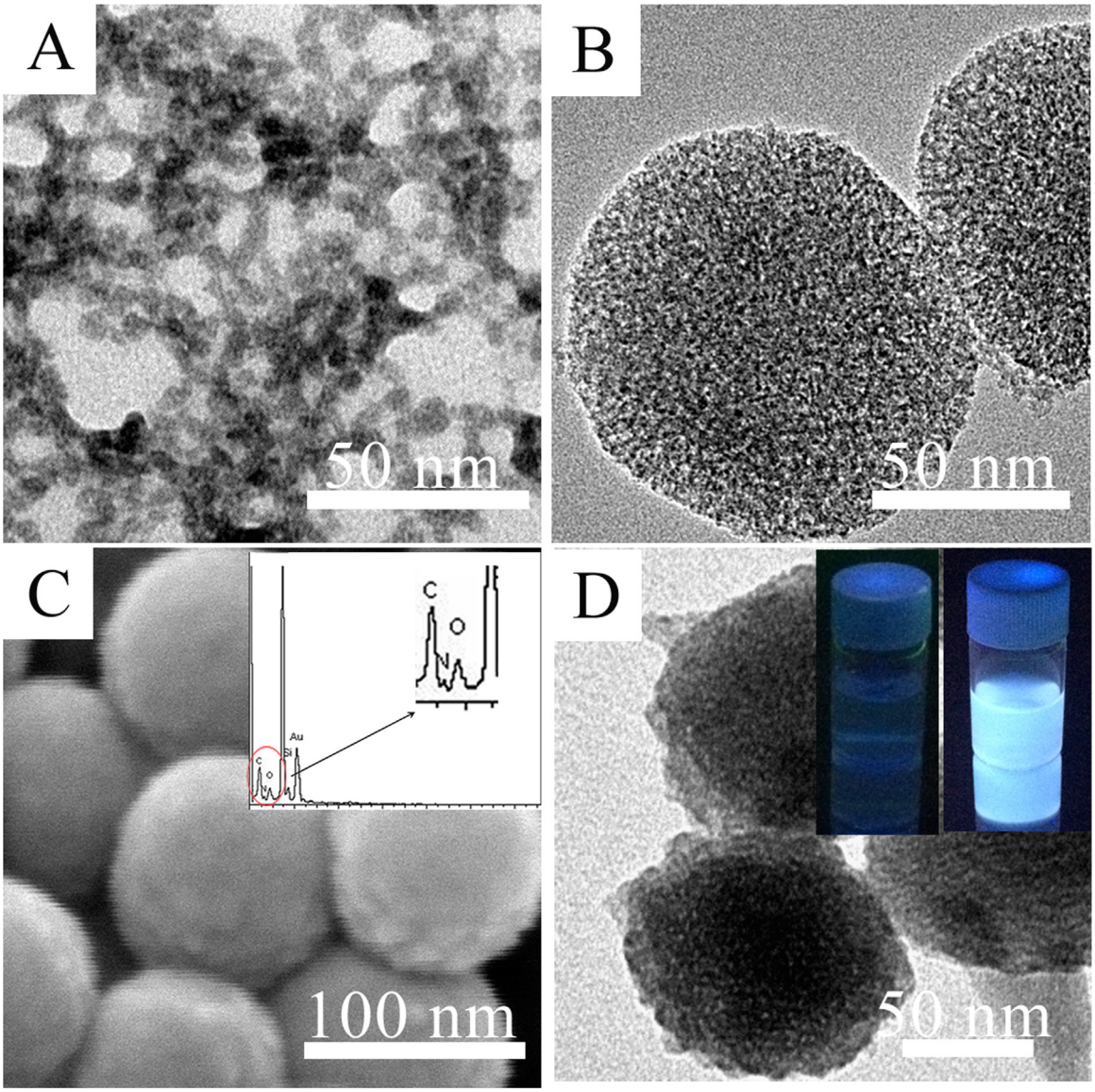

Fig. 2. (A) TEM images of NGQDs. (B) TEM images of $MPSiO_2$. (C) SEM image of $MPSiO_2$/NGQDs. Inset: EDS images. (D) TEM images of $MPSiO_2$/NGQDs. Inset: fluorescence photograph of $MPSiO_2$ (left) and $MPSiO_2$/NGQDs (right).

fluorescence excited by an UV lamp (inset).

The morphology and microstructure of $MPSiO_2$, $MPSiO_2$/NGQDs were elucidated by SEM and TEM observations (Fig. 2). The diameters of the as-synthesized $MPSiO_2$ were about 100 nm (Fig. 2B). The TEM image of $MPSiO_2$ was shown in Fig. 2B with rough surface. Obvious multilayer and pores could be seen in SiO_2, and this multilayer porous structure improved the immobilized amount of NGQDs. Fig. 2C and D showed SEM and TEM image of MPSiO2/NGQDs nanocomposite. Comparing with Fig. 2B and D, we could see that the surface texture of $MPSiO_2$ changed after NGQDs were bonded to $MPSiO_2$. $MPSiO_2$/NGQDs showed strong blue emission by an UV lamp (inset in Fig. 2D), which confirmed that NGQDs

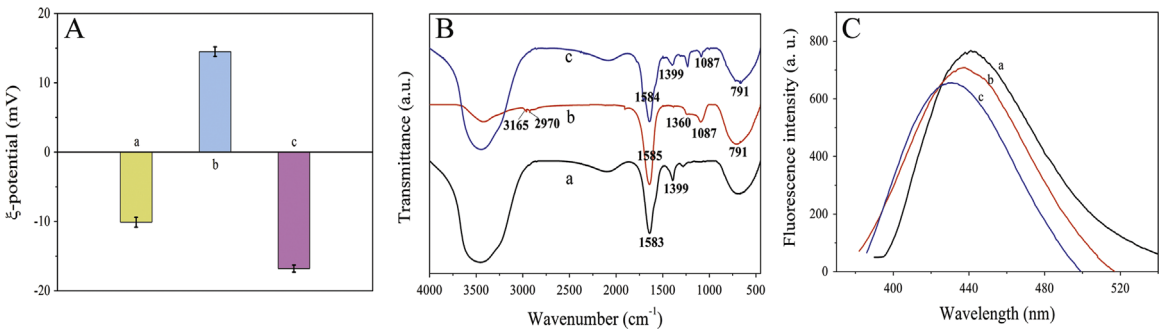

Fig. 3. (A) Value of ζ-potentials during the assembly process. The bars represent (a) pure NGQDs, (b) APTES-$MPSiO_2$ and (c) $MPSiO_2$/NGQDs. (B) FT-IR spectra of (a) pure NGQDs, (b) APTES-$MPSiO_2$ and (c) $MPSiO_2$/NGQDs. (C) Fluorescence spectra of (a) NGQDs, (b) $MPSiO_2$/NGQDs and (c) $MPSiO_2$/NGQDs-DNA.

were successfully connected to the $MPSiO_2$. The EDS analysis (insert in Fig. 2C) showed that the sample consisted of Si, N, O and C elements, which was further demonstrated that $MPSiO_2$/NGQDs was synthesized successfully.

The ζ-potential of NGQDs, APTES-$MPSiO_2$ and $MPSiO_2$/NGQDs were shown in Fig. 3A, respectively. The NGQDs were negatively charged with a ζ-potential of −10.1 mV, whereas the ζ-potential of APTES-$MPSiO_2$ was +14.5 mV due to the amino groups. After the modification of negatively charged NGQDs, the ζ-potential decreased to −16.8 mV. The results were consistent with the successful fabrication of $MPSiO_2$/NGQDs.

To further investigate the surface charge of the $MPSiO_2$/NGQDs in the fabrication process, the FT-IR spectra of NGQDs, APTES-$MPSiO_2$ and $MPSiO_2$/NGQDs were shown in Fig. 3B. In the curve of NGQDs, the NGQDs only showed C-O (carboxy) asymmetric stretching and asymmetric bending vibrations peak at 1583 cm^{-1} and 1399 cm^{-1} and O-H group (carboxy) stretching peak at 3458 cm^{-1}, which showed that the obtained NGQDs contained –COOH and –OH groups. In the curve of APTES-$MPSiO_2$, the peaks of 3165 cm^{-1} and 2970 cm^{-1} were attributed to asymmetric vibrations of N-H of the $–NH_3$. Moreover, several absorption bands at 791, 1087, 1360, and 1585 cm^{-1} were assigned to the Si-O-Si, (Si-O)n, C-N, and N-H stretching or bending vibrations, respectively, which testified that APTES moieties had been successfully grafted onto the surface of $MPSiO_2$ during the modification process. After assemble the NGQDs on the $MPSiO_2$, the corresponding absorption peaks of $–NH_2$ became very weak or disappeared, because the $–NH_2$ groups reacted with COO^-. In addition, the characteristic peaks of COO^- group around 1584 cm^{-1} and 1399 cm^{-1} were existed which were further used to immobilized DNA.

Fluorescence measurements of NGQDs, $MPSiO_2$/NGQDs and $MPSiO_2$/NGQDs-DNA, respectively, were shown in Fig. 3C. As presented in Fig. 3C, NGQDs showed an intense and sharp emission band at 441 nm, whereas a slight blue shift of the maximum emission wavelength from 441 to 437 nm and 437–431 nm were observed after $MPSiO_2$ and DNA functionalization, respectively. Given the structural characteristics of the $MPSiO_2$/NGQDs, this blue shift of the emission band in the fluorescence spectrum could be attributed to the interaction between NGQDs and $MPSiO_2$ and the change of NGQDs' size, indicating the successful preparation of $MPSiO_2$/NGQDs and $MPSiO_2$/NGQDs-DNA.

3.3. Possible mechanism for the fluorescence behaviors

A mechanism of this biosensor was shown in Scheme 1. The underlying chemistry involved in our design is based on a process similar to the Fenton reaction. When H_2O_2 was present, •OH was produced during FA-pPdAu/GO and NGQDs-catalyzed oxidation of H_2O_2 (Fig. S8). •OH was believed to be the main contributor to overall oxidative DNA damage, through hydrogen abstraction from the deoxyribose phosphate backbone (Zhang et al., 2011). Thus, the •OH attacked the $MPSiO_2$/NGQDs-labeled long ssDNA, underwenting irreversible self-cleavage after the introduction of •OH and producing the $MPSiO_2$/NGQDs-linked DNA fragment. Due to the weak interaction between FA-pPdAu/GO and the $MPSiO_2$/NGQDs-linked DNA fragment, the $MPSiO_2$/NGQDs-linked DNA fragment was released from the FA-pPdAu/GO surface and the fluorescence of the system was recovered. Whereas, in the absence of H_2O_2, the Fenton reaction did not occur, and the long ssDNA was not damaged, which resulted in strong binding between the long ssDNA and FA-pPdAu/GO via π-π stacking interactions. So, the fluorescence intensity of the system should gradually increase with increasing concentration of H_2O_2 in the system.

3.4. The H_2O_2 standard solution concentration-dependent fluorescence intensity

we firstly evaluated the fluorescence quenching capability upon different concentrations of the prepared FA-pPdAu/GO. As shown in Fig. 4A and B, the effect of the concentration of FA-pPdAu/GO was studied over the range between 5 and 125 μg mL^{-1}. We found that the fluorescence intensity decreased with the increase of FA-pPdAu/GO concentration which indicated that probes were adsorbed on the surface of FA-pPdAu/GO efficiently. And The as-prepared nanoassembly was found to give very weak fluorescence (100 μL $MPSiO_2$/NGQDs-DNA probes achieve 96.03% quenching of the fluorescence by measuring fluorescence spectra in the presence of 125 μg mL^{-1} FA-pPdAu/GO), therefore, 125 μg mL^{-1} FA-pPdAu/GO was used for this research. The high quenching efficiency was mainly attributed to the π-π stacking interaction between GO and probe, the strong interactions between the GO and NGQDs and the high stability and water-solubility made GO a good quencher for this cells detection probe design.

We next demonstrated the fluorescence recovery upon addition of H_2O_2 standard solution of various concentrations. Under the optimal conditions (the details can be found in the Fig. S9 and Fig. S10), our constructed cancer cells immobilized HC-μPADs by using folic acid as a recognition element were employed to obtain the varied fluorescence values towards various concentrations of H_2O_2. Firstly, we assessed the ability of HC-PFAD to visualize quantitative determination H_2O_2. As could be seen in Fig. 4D, the color increased with the concentration increasing of H_2O_2 under UV lamp, which indicated the HC-PFAD particularly attractive for visually H_2O_2 sensing. Then, the dynamic range for detecting H_2O_2 with the fluorescence method were also examined. As could be seen in Fig. 4C and D that the fluorescence intensity gradually increased with increasing the concentration of H_2O_2. A good linear relationship between the fluorescence intensity and logarithm of H_2O_2 concentrations was obtained in the range of 0.3 nM to 1.0 mM. The linear regression equations for H_2O_2 was expressed as follows: $\Delta F = 97.53 \log[cH_2O_2(nM)] + 113.13$ with the correlation coefficient of R=0.9988. The detection limit was estimated to be 0.1 nM (at a signal/noise ratio of 3), which was much lower than those reported previously (Table S1).

3.5. Cytotoxicity Investigation of the Nanoprobe

For practical biomedical applications, a nanostructured probe and paper-based nanoplatform should not interfere with the metabolism of the living system. Therefore, cytotoxicity of the $MPSiO_2$/NGQDs-DNA and paper-based nanoplatform toward MCF-7 cells as the model was evaluated using the standard cell MTT assay by the use of the calcein-AM (a living cell dyes) and propidium iodide (PI, a dead cell dyes). Firstly, cytotoxicity of the paper-based nanoplatform was performed, for the viable cell screening, the captured MCF-7 (10^6 cells mL^{-1}) was cultured in situ in paper-based nanoplatform for 1 h, 4 h, 7 h, 10 h or 12 h, respectively. Then, Media in the dishes were discarded and cells were gently rinsed twice with PBS. 0.5 mM of the calcein-AM solution was added into the dishes and incubated for 30 min at 37 °C. The results of the fluorescent imaging technique were shown in Fig. 5A. It can be observed that the fluorescent intensities increased gradually, with the incubation time varying from 1 h to 12 h. Fig. 5B showed that the entire fluorescent imaging was almost no PI-positive cells after the cultivation of 8 h. This result showed that the paper-based nanoplatform had no obvious cytotoxic effect on the living system, because of the good biocompatibility of the FA-pPdAu/GO and cellulose fibers. Next, the cytotoxicity of $MPSiO_2$/NGQDs-DNA was also studied, MCF-7 cancer cells were incubated with $MPSiO_2$/NGQDs-DNA. After 8 h of incubation, the cells were

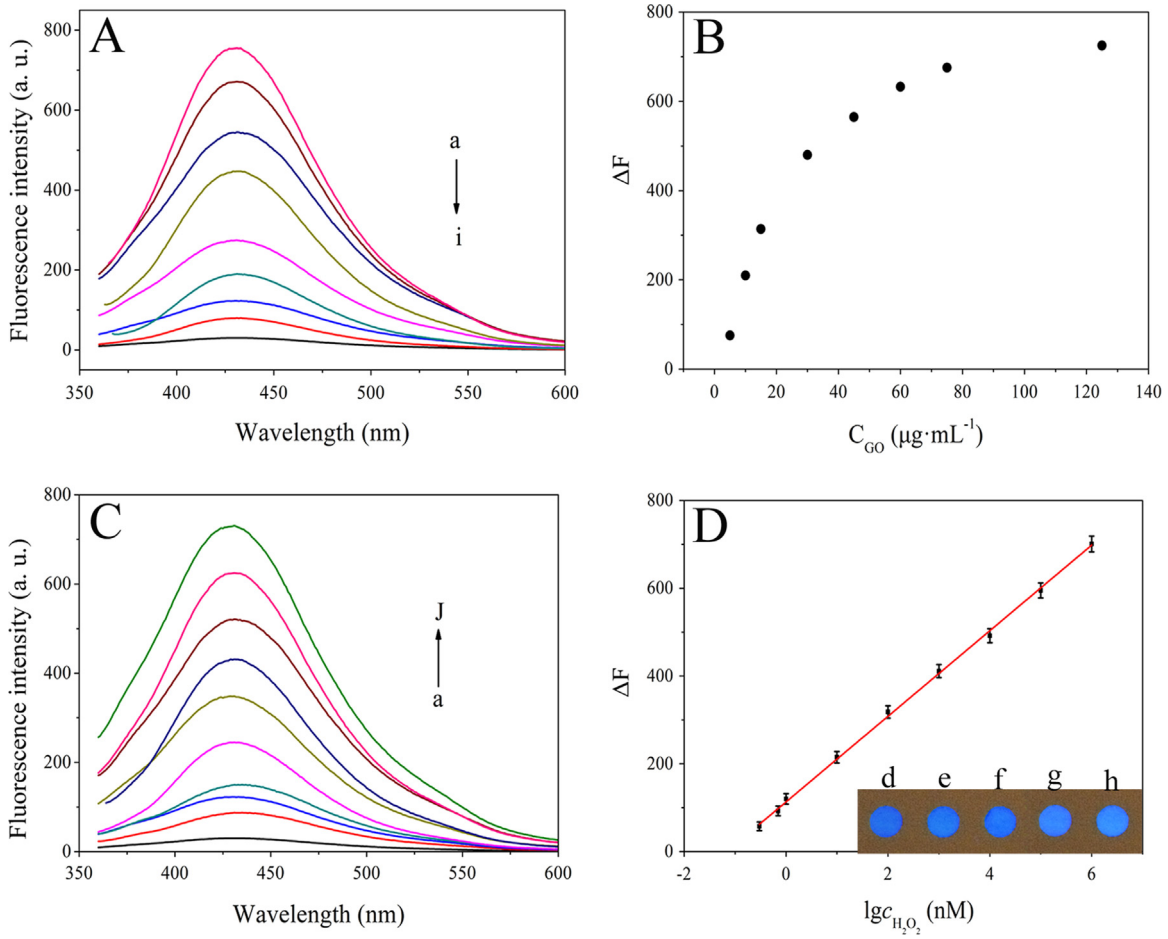

Fig. 4. (A) Changes in the fluorescence spectra and (B) the curve of quenched fluorescence intensity of probe in PBS solution (pH 7.4) with an increasing concentration of FA-pPdAu/GO, with concentrations of 0, 5, 10, 15, 30, 45, 60, 75, 125 μg mL^{-1}. (C) The fluorescence responses of the HC-PFAD towards various concentrations of H_2O_2 in 10 mM PBS (pH 7.4); (D) (upper) calibration curve for H_2O_2 determination; (lower) Fluorescence photographs of probes incubated with different concentrations of H_2O_2.

stained for 15 min at 37 °C by added 1 mL of the calcein-AM and PI solution. As shown in Fig. 5C, MCF-7 cancer cells showed a good living morphology and. It should be noted that, $MPSiO_2$/NGQDs-DNA have no apparent effect on cancer cells. Above all, these results suggested that the materials as-prepared have no apparent harm to cells.

3.6. *Measuring the flux of H_2O_2 releasing from MCF-7 cells*

The developed method could be also used for evaluating the flux of H_2O_2 releasing from the cells on application of different stimuli such as fMLP, ADP, and AA, which were reported to induce the generation of H_2O_2 in cells (Yang et al., 2013). The flux of H_2O_2 from the cells increased in the order ADP, AA, fMLP, and PMA (each at a concentration of 100 ng mL^{-1}) (Fig. 5E), which was indicative of a stimulus type-dependent manner. Moreover, the common coexisting ROS and compounds in biological systems such as OCl–, NO·, ONOO– and AA, do not affect the catalytic oxidative of H_2O_2 since they result in a negligible signal (Fig. S11), demonstrating that the biosensor had good selectivity and anti-interference ability.

PMA is such a stimulant, which induces H_2O_2 generation in cells with a more consistent and durable chemotactic response. As the result of stimulation by PMA, a respiratory burst occurs with H_2O_2 as the end product. The endogenous generation of H_2O_2 in MCF-7 cells was evaluated (Fig. S12) and the flux of H_2O_2 release from the cells was measured with the use of the developed method. When MCF-7 cells (10^6 cells mL^{-1}, 10 μL) were stimulated by PMA (100 ng mL^{-1}, the details can be found in the Fig. S13), the fluorescence response increased suddenly (Fig. 5D), turning out that a large amount of H_2O_2 being released from the cells. Then a stable fluorescence response was reached (6s, Fig. S14), featuring the end of the event. The fluorescence intensity was about 445.1, which corresponded to 25.23 mM H_2O_2 based on the calibration equation depicted in Fig. 4. The amount of $(2.5 \pm 0.2) \times 10^{-15}$ mol for H_2O_2 releasing from each cell was obtained based on further calculations. These results suggested that the method could be used in determining the releasing flux of H_2O_2 from cells and in studying its dynamic process. Compared with the fluorescence intensity for H_2O_2 released from cells by GO in Fig. 5D (curve b and d), our developed fluorescent nanoplatform exhibited a higher fluorescence signals.

The capture of cancer cells on the HC-PFAD using folic acid also allowed it to be used for in situ anticancer drug screening. Doxorubicin (Dox) and etoposide are active chemotherapeutic agents used in clinical oncology. And Dox is a key adjuvant drug for breast cancer treatment, which triggers apoptosis through several mechanisms. Thus, to confirm the screening of anticancer drugs in this HC-PFAD, Dox was selected as the model drug for the induction of MCF-7 cells apoptosis. For the anticancer drug screening, the captured MCF-7 cells (10^5 cells mL^{-1}, 10 μL) were subsequently treated with Dox for 18 h to obtain drug-treated MCF-7/HC-PFAD. Using fluorescein isothiocyanate labeled annexin-V as the fluorescent bioprobes, the Dox induced apoptosis of MCF-7 cells was demonstrated by the fluorescent imaging technique in this cancer cell modified HC-PFAD. The fluorescence intensity

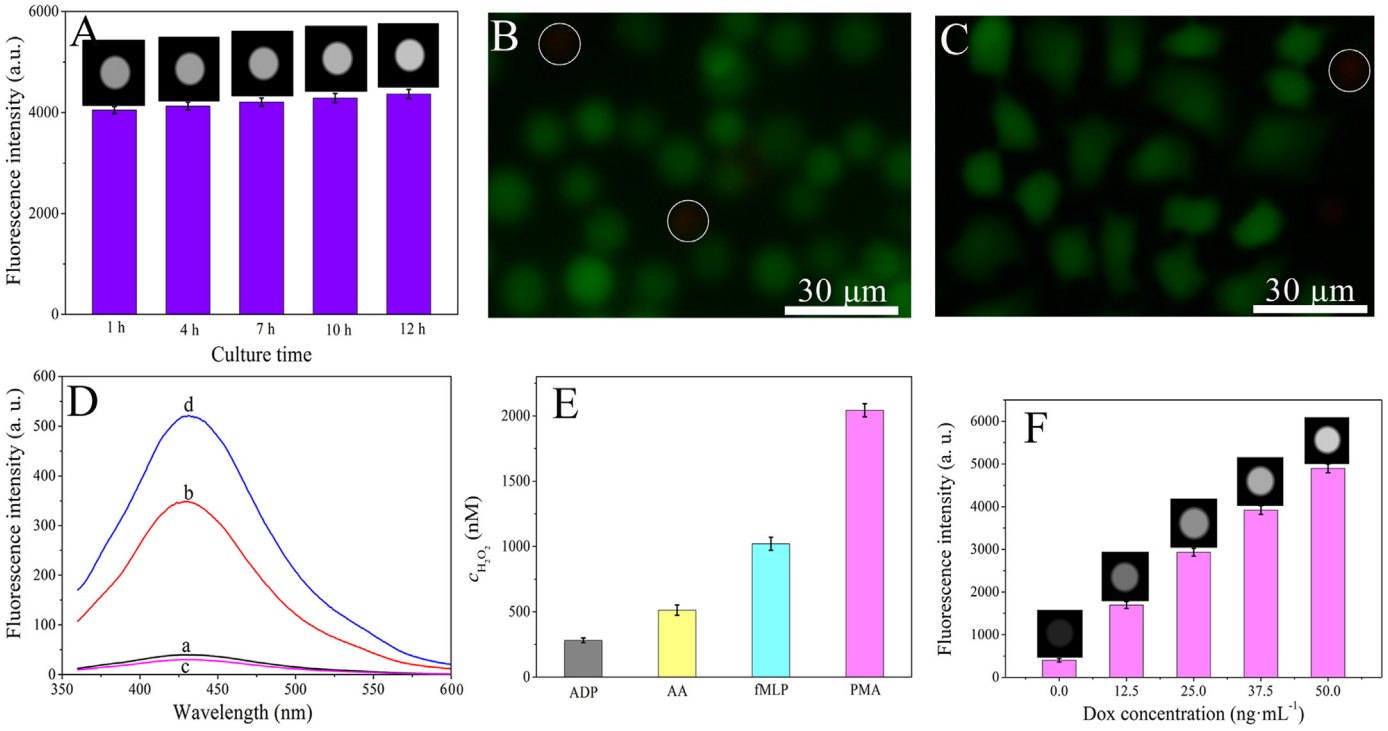

Fig. 5. (A) Fluorescent evaluation (B) Fluorescence imaging of paper-based nanoplatform cytotoxicity. (C) Fluorescence imaging of MPSiO$_2$/NGQDs-DNA cytotoxicity. (D) Fluorescence responses obtained with the HC-PFAD by GO in 10 mM PBS without (a) and with 100 ng mL^{-1} PMA or by pPdAu/GO in 10 mM PBS without (c) and with 100 ng mL^{-1} PMA (d). (E) Comparison of the fluorescence intensity for H_2O_2 released from cells, induced by 100 ng mL^{-1} ADP, AA, fMLP, and PMA. (F) Fluorescent evaluation of MCF-7 cell apoptosis after incubation with different concentrations of Dox.

validated the amount of apoptotic MCF-7 cells and the results of the fluorescent imaging technique were shown in Fig. 5F. Obviously, the drug-induced variations of fluorescence intensities were also observed in a concentration dependent manner.

4. Conclusion

In conclusion, we have developed a novel 3D HC-PFAD for a highly sensitive determination of H_2O_2 release from living cancer cells based on FA-pPdAu/GO and NGQDs-catalyzed oxidation of H_2O_2 and the cleavage of DNA by as-generated hydroxyl radicals (●OH). It was the first time that combined fluorescence with cytosensing for the detection of H_2O_2 in HC-μPADs. This developed 3D HC-PFAD displayed a low detection limit and wide linear range for quantification of H_2O_2 with desirable reproducibility and stability. Furthermore, this sensor has exhibited excellent biocompatibility and the capability of in situ and simple anticancer drug screening, and could be used for visually determined the flux of H_2O_2 from the cells. This fluorescent nanoplatform could also be easily applied for other substrate detection, involving the generation of H_2O_2, such as glucose, choline, and so on. Therefore, we anticipate that this versatile, practical, and convenient HC-PFAD will provide a significant alternative protocol for biological and clinical diagnosis applications.

Acknowledgements

This work was financially supported by Special Fund for Shandong Independent Innovation and Achievements Transformation (No. 2014ZZCX02703), the National Natural Science Foundation of China (21575051) and the Nature Science Foundation of Shandong Province, China (ZR2015JL006).

Appendix A. Supporting information

Supplementary data associated with this article can be found in the online version at http://dx.doi.org/10.1016/j.bios.2016.03.076.

References

Belousov, V.V., Fradkov, A.F., Lukyanov, K.A., Staroverov, D.B., Shakhbazov, K.S., Terskikh, A.V., Lukyanov, S., 2006. Nat. Methods 3, 281–286.
Carrilho, E., Martinez, A.W., Whitesides, G.M., 2009. Anal. Chem. 81, 7091–7095.
Chang, H., Wang, X., Shiu, K.K., Zhu, Y., Wang, J., Li, Q., Chen, B., Jiang, H., 2013. Biosens. Bioelectron. 41, 789–794.
Chou, S.S., De, M., Luo, J., Rotello, V.M., Huang, J., Dravid, V.P., 2012. J. Am. Chem. Soc. 134, 16725–16733.
Cocheme, H.M., Logan, A., Prime, T.A., Abakumova, I., Quin, C., McQuaker, S.J., Patel, J.V., Fearnley, I.M., James, A.M., Porteous, C.M., Smith, R.A., Hartley, R.C., Partridge, L., Murphy, M.P., 2012. Nat. Protoc., 7946–7958.
Dickinson, B.C., Chang, C.J., 2008. J. Am. Chem. Soc. 130, 9638–9639.
Ge, L., Wang, P.P., Ge, S.G., Li, N.Q., Yu, J.H., Yan, M., Huang, J.D., 2013. Anal. Chem. 85, 3961–3970.
He, S., Song, B., Li, D., Zhu, C., Qi, W., Wen, Y., Wang, L., Song, S., Fang, H., Fan, C.A., 2010. Adv. Funct. Mater. 20, 453–459.
Kanvah, S., Joseph, J., Schuster, G.B., Barnett, R.N., Cleveland, C.L., Landman, U., 2010. Acc. Chem. Res. 43, 280–287.
Lai, C.Y., Trewyn, B.G., Jeftinija, D.M., Jeftinija, K., Xu, S., Jeftinija, S., Lin, V.S.Y., 2003. J. Am. Chem. Soc. 125, 4451–4459.
Lee, W.R., Kim, M.G., Choi, J.R., Park, J.I., Ko, S.J., Oh, S.J., Cheon, J., 2005. J. Am. Chem. Soc. 127, 16090–16097.
Li, L., Wu, G., Yang, G., Peng, J., Zhao, J., Zhu, J.J., 2013. Nanoscale 5, 4015–4039.
Lim, B., Xia, Y.N., 2011. Angew. Chem. Int. Ed. 50, 76–85.
Lin, L.P., Song, X.H., Chen, Y.Y., Rong, M.C., Zhao, T.T., Wang, Y.R., Jiang, Y.Q., Chen, X., 2015. Anal. Chim. Acta 869, 89–95.
Lin, L., Rong, M., Luo, F., Chen, D., Wang, Y., Chen, X., 2014. TrAC Trends Anal. Chem. 54, 83–102.
Lippert, A.R., Van de Bittner, G.C., Chang, C.J., 2011. Acc. Chem. Res. 44, 793–804.
Liu, H., Crooks, R.M., 2012. Anal. Chem. 84, 2528–2532.
Liu, S., Nie, H., Jiang, J., Shen, G., Yu, R., 2009. Anal. Chem. 81, 5724–5730.
Martinez, A.W., Phillips, S.T., Butte, M.J., Whitesides, G.M., 2007. Angew. Chem. Int. Ed. 46, 1318–1320.
Martinez, A.W., Phillips, S.T., Whitesides, G.M., 2010. Anal. Chem. 82, 3–10.
Nery, E.W., Kubota, L.T., 2013. Anal. Bioanal. Chem. 405, 7573–7595.

Renault, C., Anderson, M.J., Crooks, R.M., 2014. J. Am. Chem. Soc. 136, 4616–4623.
Renault, C., Li, X., Fosdick, S.E., Crooks, R.M., 2013. Anal. Chem. 85, 7976–7979.
Sanford, A.L., Morton, S.W., Whitehouse, K.L., Oara, H.M., Lugo-Morales, L.Z., Sombers, L.A., 2010. Anal. Chem. 82, 5205–5210.
Shang, L., Dong, S.J., 2009. Anal. Chem. 81, 1465–1470.
Shibutani, S., Takeshita, M., Grollman, A.P., 1991. Nature 349, 431–434.
Su, L., Feng, J., Zhou, X.M., Ren, C.L., Li, H.H., Chen, X.G., 2012. Anal. Chem. 84, 5753–5758.
Tang, Y.F., Allen, B.L., Kauffman, D.R., Star, A., 2009. J. Am. Chem. Soc. 131, 13200–13201.
Whitesides, G.M., 2006. Nature 442, 368–373.
Yang, Y., Zhou, J.W., Zhang, Y.S., Zou, Q., Zhang, X.H., Chen, J.H., 2013. Sens. Actuators B 182, 504–509.
Yetisen, A.K., Akram, M.S., Lowe, C.R., 2013. Lab Chip 13, 2210–2251.
Zhang, H., Jin, M., Wang, J., Li, W., Camargo, P.H.C., Kim, M.J., Yang, D., Xie, Z., Xia, Y., 2011. J. Am. Chem. Soc. 133, 6078–6089.
Zhang, L.N., Deng, H.H., Lin, F.L., Xu, S.W., Weng, S.H., Liu, A.L., Lin, X.H., Xia, X.H., Chen, W., 2014. Anal. Chem. 86, 2711–2718.
Zhang, Y., Wu, C., Zhou, X., Wu, X., Yang, Y., Wu, H., Guo, S., Zhang, J., 2013. Nanoscale 5, 1816–1819.